Journal of Alloys and Compounds 854 (2021) 156169

Contents lists available at ScienceDirect

Journal of Alloys and Compounds

journal homepage: http://www.elsevier.com/locate/jalcom

Electron transport and thermoelectric properties of ZnO ceramics doped with Fe

A.K. Fedotov [a], A.V. Pashkevich [a, b], J.A. Fedotova [a], A.S. Fedotov [b], T.N. Kołtunowicz [c, *], P. Zukowski [c], Ali Arash Ronassi [d], V.V. Fedotova [e], I.A. Svito [b], M. Budzyński [f]

[a] Institute for Nuclear Problems of Belarusian State University, 220040, Minsk, Belarus
[b] Belarusian State University, 220030, Minsk, Belarus
[c] Lublin University of Technology, 20-618, Lublin, Poland
[d] Payame Noor University, Tehran, Iran
[e] Practical-Scientific Center of NASB on Material Science, 220078, Minsk, Belarus
[f] Maria Curie-Sklodowska University, 20-031, Lublin, Poland

ARTICLE INFO

Article history:
Received 22 May 2020
Received in revised form
19 June 2020
Accepted 22 June 2020
Available online 12 September 2020

Keywords:
Electron transport
Thermoelectric properties
ZnO
Seebeck effect

ABSTRACT

Currently, special attention is paid to the search for new ceramic materials based on wide-gap oxides, as well as to the study of their structure and properties with a view to their application in various areas of electronic and optoelectronic industry.

Conventional double-step ceramic technology has been used to obtain samples in this experiment. After compacting at the pressure of 6 GPa of ZnO and ZnO-Fe_xO_y powders in different weight relations, the samples were subjected to the procedure of synthesis at 1173 K for 2 h and then to the annealing at 1473 K for 3 h on air.

The samples structure was investigated by the Scanning Electron Microscopy (SEM), Energy-dispersive X-ray Spectroscopy (EDX), X-ray Diffraction (XRD) and Raman spectroscopy methods. Temperature dependences of resistivity, magnetoresistance, Hall and Seebeck effects were experimentally studied in the range from 4 to 700 K.

As the experiments have shown, the size of grains in the obtained ceramic samples after synthesis was in submicron range. An XRD study showed the saving of the wurtzite structure in $Zn_{1-\delta}Fe_\delta O$ solid solutions where $0.66 < \delta < 0.81$ at. % regardless of the type of the doping agent. At the same time, the replacement of zinc by iron atoms led to the contraction of the ZnO lattice.

All the samples studied (ZnO and $Zn_{1-\delta}Fe_\delta O$) demonstrate n-type conductivity. The temperature dependencies of resistivity have shown two specific features: the presence of energy level about 0.35 eV below the conduction band bottom for the doped ceramic samples (unknown in literature) and conductance with the changing activation energy at temperatures below 200 K for the undoped ZnO ceramic samples. Seebeck coefficient increased by100–150% with doping due to growth of electron concentration. Some model concepts about scattering mechanisms and reasons of Seebeck effect enhancement have been developed.

1. Introduction

For many years special attention is paid to the search for new ceramic materials based on wide-gap oxides, as well as to the study of their structure and properties with a view to their application in various areas of electronic and optoelectronic industry. This forces to study correlations between structure and properties of composite ceramics, as well as striving for their cost-effective production technologies [1]. Such ceramic materials have a number of advantages compared with polycrystalline and epitaxial films,

* Corresponding author.
E-mail addresses: fedotov@bsu.by (A.K. Fedotov), alexei.paschckevich@yandex.by (A.V. Pashkevich), julia@hep.by (J.A. Fedotova), fedotov.alehandro@gmail.com (A.S. Fedotov), t.koltunowicz@pollub.pl (T.N. Kołtunowicz), p.zhukowski@pollub.pl (P. Zukowski), a_ronassi@yahoo.com (A.A. Ronassi), fedotova@physics.by (V.V. Fedotova), ivansvito184@gmail.com (I.A. Svito), budzyn@poczta.umcs.lublin.pl (M. Budzyński).

https://doi.org/10.1016/j.jallcom.2020.156169
0925-8388/

single crystals and other types of ZnO-based materials obtained using more expensive technologies. Ceramic technologies make it possible to manufacture products of various shapes and sizes, varying their morphology, structural and phase state, which allows to control their functional properties by changing the granules sizes in the initial powder mixtures; temperatures, duration and atmosphere of synthesis and the following heat treatments, as well as the type of doping agents [2–4]. Currently, various methods of preparing materials on the basis of ZnO are used worldwide, such as chemical vapor deposition [5–10], atomic layer deposition [11–13], sputtering [14–16], liquid-phase methods for synthesizing ZnO nanowires [17] or nanoparticles [18,19].

Using ceramic materials based on iron-doped zinc oxide, it is possible to create both traditional (for example, varistors [2]) and completely new types of devices. For example, by doping ZnO with magnetic impurities, it is possible to realize electronic, optical, magnetic and other properties controlled by a magnetic field [20–23]. Yet one application of ZnO-based composite ceramics is related to production of thermoelectric converters (TEC) [24,25]; however, this requires increasing electrical conductivity and reduction of materials thermal conductivity.

Analysis of the literature suggests that single crystals, polycrystalline films, nanostructured powders and zinc oxide-based wires have been studied in sufficient detail. At the same time, based on ZnO composites, synthesized by ceramic technologies, are far from being fully studied (probably, with the exception of varistor ceramics [2]). So, the aim of the work is to study the influence of structure, phase and chemical composition on electric and thermoelectric properties of ZnO-based ceramics when they are doped with iron using different types of Fe_xO_y ($x = 1, 2$ and $y = 1, 2, 3$) alloying agents.

2. Experimental

To obtain samples we used conventional double-step ceramic technology. After compacting at pressure of 6 GPa of ZnO and ZnO-Fe_xO_y powders with the weight relation $(ZnO)_{90}(Fe_xO_y)_{10}$, the samples were subjected to the procedure of synthesis at 900 °C for 2 h and then to the grinding into powder again, compacting (in the form of tablets with the diameter of 10–18 mm and thickness of 2–5 mm) and annealing at 1200 °C for 2 h in air. The annealed tablets were cooled in the furnace at the speed of 200–300 K/h.

The structural characterization of ceramic samples was carried out at room temperature by X-ray diffraction analysis (XRD) with Cu-K_α radiation in the automated unit DRON-3M. The X-ray patterns were processed using the FullProf code based on the Rietveld method for profile analysis [26]. The scanning step in the 2θ angles was 0.03°, and the exposure time about 5 s.

The scanning electron microscopy (SEM) in the mode of secondary electrons using the devices LEO 1455VP (Oxford Instruments, London, Great Britain) and Tescan Vega 3LMU (Tescan, Brno, Check Republic) was applied to measure grains' form and sizes. To measure concentrations of chemical elements, the energy-dispersive X-ray (EDX) analysis to be contained in SEM was used. As the measurements have shown, at mean Fe content in ceramic about (1–3) at. % the Fe concentration in solid solutions $Zn_{1-\delta}Fe_\delta O$ was about $\delta \approx (0.66–0.87)$ at. %.

To detect the porosity of the samples studied, we used the microscope Olimpus GX41 (Olimpus, Tokyo, Japan) supplied with the Auto Scan 005 software. In the studied samples, porosity was between 14.6% for the undoped ZnO and 16.5%–18.3% for the $(ZnO)_{90}(Fe_xO_y)_{10}$.

Nuclear gamma resonance (NGR) spectroscopy was carried out in a temperature range of 20–300 K using an MS4 (SEE Co) Mössbauer spectrometer (USA). NGR spectrometry was performed on powder samples in a transducent geometry using a ^{57}Co/Rh source (20 μCi). The spectra were fitted using the MOSMOD code based on the Rankur method [27]. The values of isomer shifts β were given relatively to the α-Fe phase at room temperature.

Raman spectroscopy (RS) was performed on a Nanofinder High-End confocal spectrometer (LOTIS TII, Belarus – Japan). To excite the signal, we used a solid-state laser with the wavelength of 532 nm and the power of 20 mW). The laser radiation was focused on the surface of the sample with a 50× objective (numerical aperture of 0.8). The power of laser radiation incident on the sample surface was attenuated to 2 mW in order to avoid its thermal damage. The backscattered light was dispersed by a 600 mm^{-1} diffraction grating, which made it possible to obtain a spectral resolution no worse than 3 cm^{-1}. Spectral calibration was carried out by the lines of a gas-discharge lamp, which ensured accuracy no worse than 3 cm^{-1}. The signal accumulation time was 30 s. A cooled silicon CCD matrix was used as a photodetector.

The temperature dependences of resistivity $\rho(T)$ and the Hall constant $R_H(T)$ in ceramics were measured on rectangular samples with the width of 2–3 mm and the length of 7–10 mm cut from the described above synthesized tablets. Two silver current contacts were prepared at the butts of the samples, and two potential and two Hall contacts were prepared between the current contacts at the wide edge of every sample.

Measurements of $\rho(T)$ and $R_H(T)$ were performed on the High Field Measurement System (Cryogenic Ltd., London, Great Britain) with a closed-cycle refrigerator. The sample to be measured was mounted in a special probe containing magnet field sensor, thermometers and heaters. The probe with the mounted sample was placed inside the channel of superconducting solenoid in the cryostat of the installation and connected to an automated measuring system. The dependence of $\rho(T)$ and $R_H(T)$ was measured in the temperature range of 6–300 K and in magnetic fields of 0–8 T. The current through the sample was set by the Sub-Femtoamp Remote SourceMeter Keithley 6430 (Tektronix, USA, Beverton), which made it possible to measure the electrical resistance of the samples in the range of 100 μΩ–10 GΩ with the accuracy not worse than 0.1%. The temperature of the samples was controlled by LakeShore thermodiodes calibrated with an accuracy of 0.0005 K and having a reproducibility of 0.001 K, which allowed to stabilize and measure the temperature with the LakeShore 331 controller (Lake Shore Cryotronics, Westerville, USA). The accuracy of measuring the resistivity and the Hall constant was not worse than 5%.

The magnetic properties of composite ceramics were studied in the temperature range $T = 5–300$ K and the magnetic fields B up to 8 T by the vibration sample magnetometer (VSM) using a Quantum Design VSM-PPMS installation.

To measure differential thermos-EMF the samples were inserted in a special measuring cell with two pairs of pressure bronze contacts, between which the sample was fixed. The contacts contained measuring thermometers, which made it possible to determine the temperature with the accuracy of no worse than 0.1 K. The Seebeck coefficient was determined by differentiating the experimental dependence of the thermopower on the temperature difference on the sample under study in the temperature range 290–310 K. The accuracy of measuring the Seebeck coefficient was not worse than 10%.

3. Structure and phase composition of ceramics

As was shown by the SEM studies, after preliminary sintering (1st stage), the granule sizes in ceramics were from 1 to 5 to several tens of micrometers (see Fig. 1a–d), but after the final sintering (2nd stage) the grain dimensions decreased to the submicronic range (Fig. 1e–h).

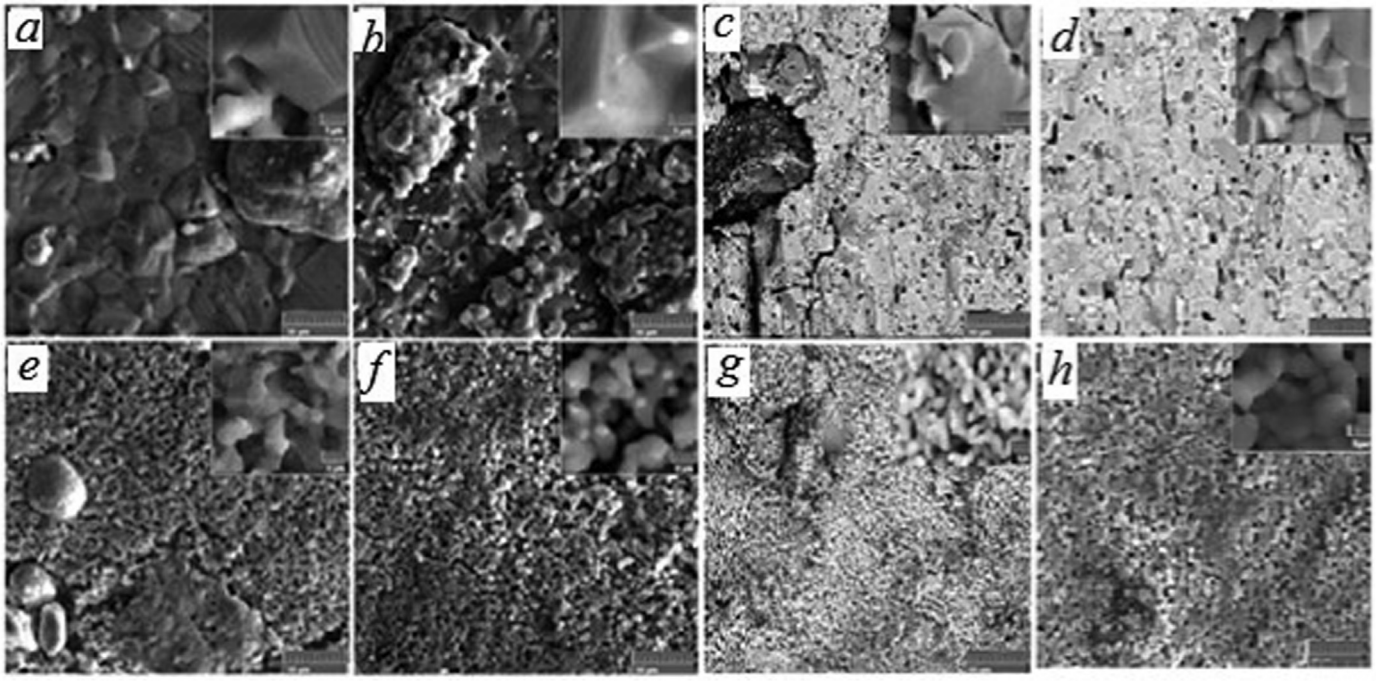

Fig. 1. Examples of SEM images of the grain structure on the cleaved surface of ceramics $(Fe_xO_y)_{10}(ZnO)_{90}$ obtained after one- (a, b, d, g) and two-stage (e, f, g, h) synthesis using FeO (a, e), α-Fe_2O_3 (b, f), Fe_3O_4 (c, g) oxides and a mixture (50 FeO + 50 Fe_2O_3) (d, h) as the doping oxides. The inserts give the SEM images of samples' sections with higher magnification.

Fig. 2 shows the XRD patterns of the undoped and doped ZnO with various types of the doping agents Fe_xO_y. The undoped ZnO ceramics display the hexagonal wurtzite structure (it is well matched with JCPDS Card No. 05-0664). The Fe-doped samples reveal at least 3 phases: the hexagonal phase of ZnO wurtzite structure, the spinel structure of $ZnFe_2O_4$ (in accordance with JCPDS Card No: 89-0951) and the FCC phases for the rests of doping agents Fe_xO_y (in accordance with JCPDS Card No: 89-0951) [28]. Therefore, the XRD method shows (Fig. 2) the prevailing of solid solutions $Zn_{1-\delta}Fe_\delta O$ with the wurtzite structure independently on the type of Fe_xO_y doping agent. According to the EDX microanalysis in SEM, that the iron content in the wurtzit matrix $Zn_{1-\delta}Fe_\delta O$ of the

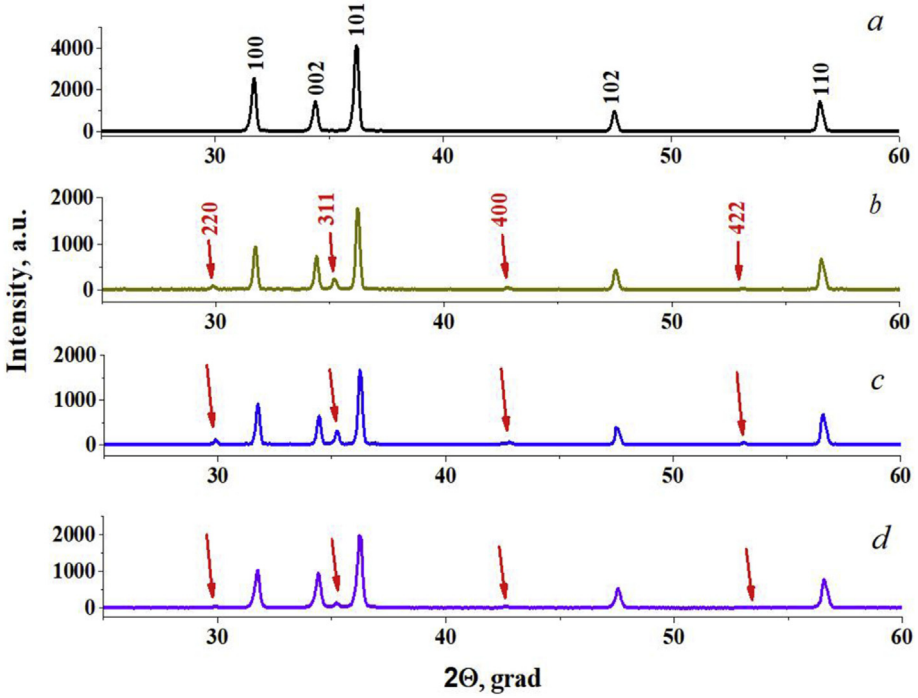

Fig. 2. Examples of XRD patterns in undoped ZnO and composite ceramics $(Fe_xO_y)_{10}(ZnO)_{90}$, obtained by the method of two-step synthesis, using different doping agents Fe_xO_y: ZnO (a), FeO (b), Fe_2O_3 (c) and Fe_3O_4 (d). Miller indices near the XRD reflexes are shown by black figures for the $Zn_{1-\delta}Fe_\delta O$ wurtzite phase, by red figures for the Fe_xO_y doping agents and by green figures for ferrite $ZnFe_2O_4$. (For interpretation of the references to colour in this figure legend, the reader is referred to the Web version of this article.)

studied ceramics was in the range of $0.30 < \delta < 0.81$ at. %.

The lattice parameters values for the $Zn_{1-\delta}Fe_{\delta}O$ wurzite phase obtained from approximation by the Rietveld method are summarized in Fig. 2. We detected some decrease in lattice parameters *a* and *c* when doping of ZnO, probably due to partial replacement of Zn ions in the wurtzite phase with iron ions. The magnitude of this lattice contraction in doped wurtzite clearly correlates with the number of oxygen atoms per unit formula of iron oxide used as a doping agent. It should also be noted that the ratio $a/c = 1.60$ is preserved for all the studied doping agents, i.e. the lattice cell itself is not distorted.

Example of the additional Fe-enriched phases fixed by the EDX method in the $(ZnO)_{90}(Fe_2O_3)_{10}$ ceramics is presented in Fig. 3 together with the SEM images. As follows from Fig. 4, in the composite ceramics, in addition to the more or less homogeneously distributed grains of $Zn_{1-\delta}Fe_{\delta}O$ solid solutions with the wurtzite structure (dark areas with $\delta < 1$ at. % in Fig. 3), there are areas with sizes up to tens of μm, which contain up to 1–3 at. % iron (light areas in Fig. 3b).

The Raman spectra of the studied ceramic samples were measured specially at several points that got either to the region of the $Zn_{1-\delta}Fe_{\delta}O$ solid solutions (Fig. 4a) or to the particles with the iron enriched phases (Fig. 4b), that were shown in Fig. 3. The comparison of the Raman lines positions in Fig. 4 with the literature data [29–34] indicates the presence of wurtzite $Zn_{1-\delta}Fe_{\delta}O$ and two cubic phases, one of which is identified as $ZnFe_2O_4$ zinc ferrite, and others can be attributed to residues of the Fe_xO_y doping agents, confirming the XRD data.

To analyze the phase transformations during the synthesis of the studied composite ceramics, we measured Mossbauer spectra for both the initial powders before compacting, as well as after two-step synthesis (Fig. 5). The NGR spectra of the initial powders are characterized mainly by a sextet, corresponding to α-Fe_2O_3 and Fe_2O_3 phases. After mixing and compaction of powders, homogenization of the iron-containing phases occurs takes place. Therefore, the NGR spectra obtained for $(ZnO)_{90}(Fe_xO_y)_{10}$ powder mixtures and for the ceramics show one doublet corresponding to iron ions Fe^{3+}.

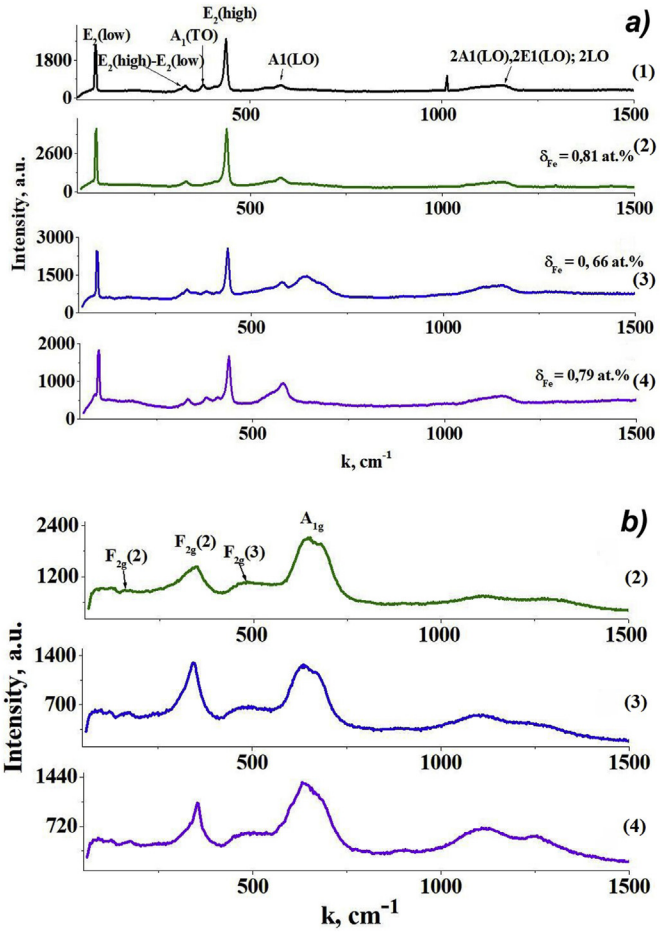

Fig. 4. Examples of Raman spectra for the wurtzite phase (a) and phases enriched by Fe (b) in composite ceramics, obtained by the method of two-stage synthesis: (1) ZnO, (2) $(ZnO)_{90}(FeO)_{10}$, (3) $(ZnO)_{90}(Fe_2O_3)_{10}$ and (4) $(ZnO)_{90}(Fe_3O_4)_{10}$.

4. Magnetic, electric and thermoelectric properties of ceramics

To analyze the magnetic properties of the iron doped ZnO-based ceramics, we selected samples of materials that correspond to the mostly different structural properties and local ordering characteristics. Fig. 6 shows the magnetization curves for *M*(*B*) of (α-$Fe_2O_3)_{10}(ZnO)_{90}$ and $(Fe_3O_4)_{10}(ZnO)_{90}$ ceramics that were produced by two-stage technology. According to XRD and Mossbauer spectra, the sample (α- $Fe_2O_3)_{10}(ZnO)_{90}$ contains large quantity of $ZnFe_2O_4$ phase (Fig. 7a) and the sample $(Fe_3O_4)_{10}(ZnO)_{90}$ has the largest amount of magnetic oxide α-Fe_2O_3 and the minimal amount of $ZnFe_2O_4$ phase (Fig. 7b).

As can be seen from Fig. 6a, (α-$Fe_2O_3)_{10}(ZnO)_{90}$ sample has paramagnetic properties at 150 K < *T* < 300 K and is predominantly

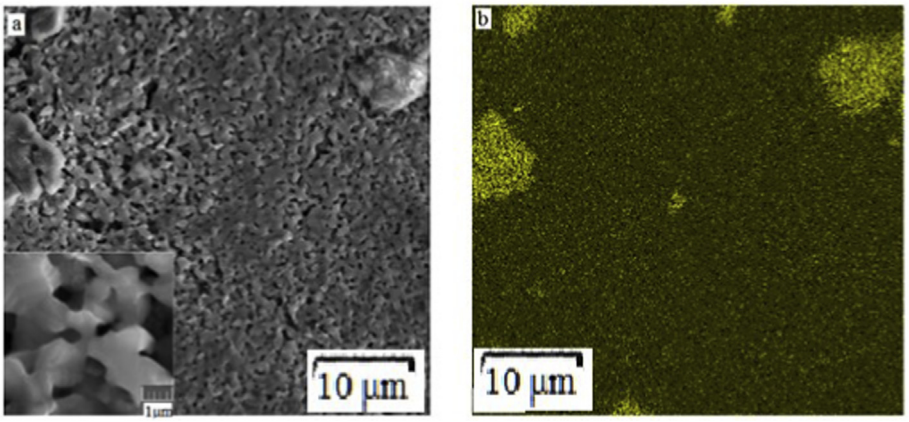

Fig. 3. SEM image (a) and EDX picture of Fe distribution (b) in the composite ceramics $(ZnO)_{90}(Fe_3O_4)_{10}$.

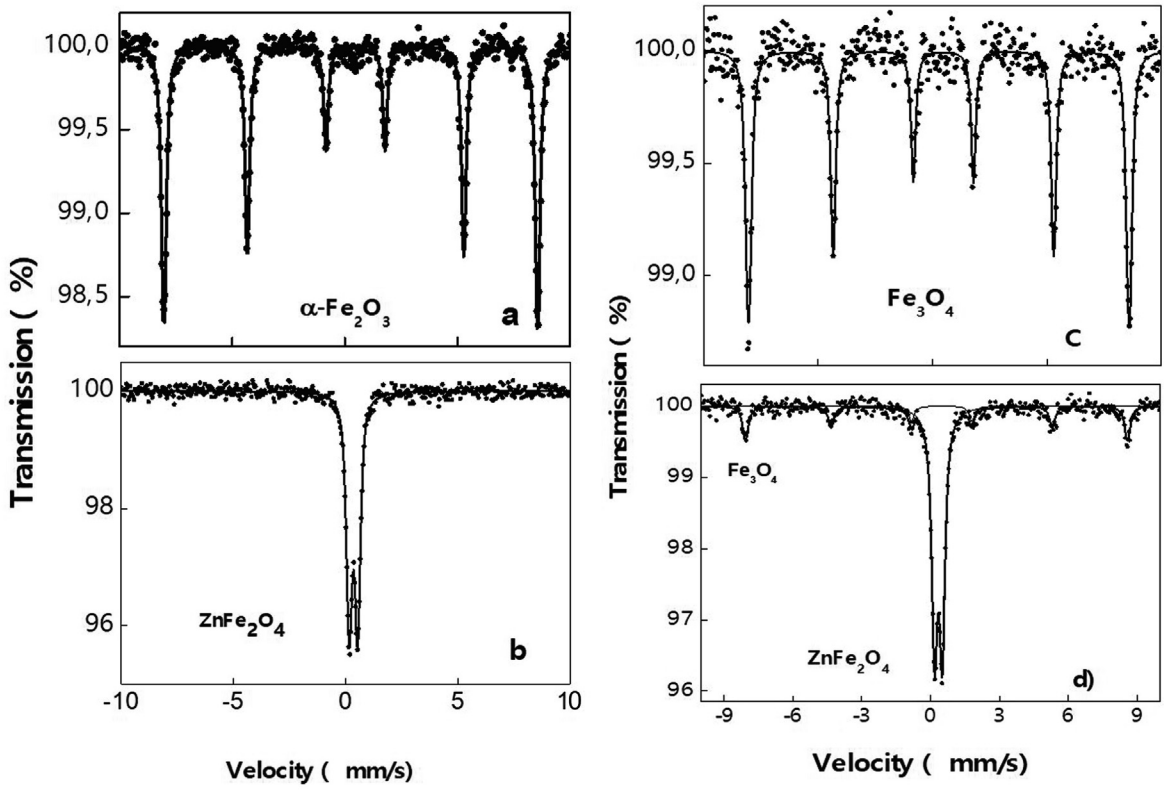

Fig. 5. Mossbauer spectra of the initial powders $(ZnO)_{90}(\alpha\text{-}Fe_2O_3)_{10}$ (*a*) and $(ZnO)_{90}(Fe_3O_4)_{10}$ (c), as well as the corresponding composite ceramics $(ZnO)_{90}(Fe_2O_3)_{10}$ (b) and $(ZnO)_{90}(Fe_3O_4)_{10}$ (d) obtained by the method of two-step synthesis.

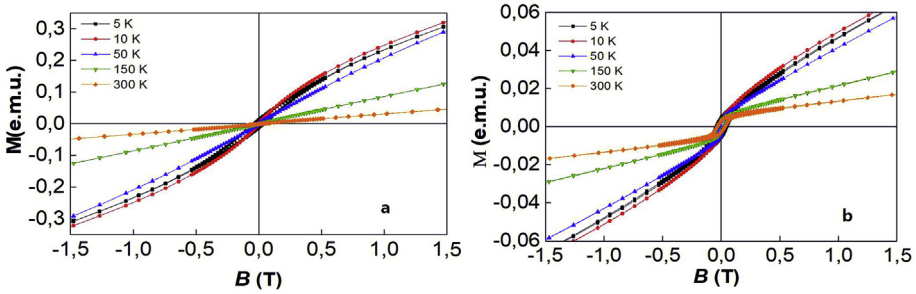

Fig. 6. Magnetization curves $M(B)$ of $(\alpha\text{-}Fe_2O_3)_{10}(ZnO)_{90}$ (a) and $(Fe_3O_4)_{10}(ZnO)_{90}$ (b) ceramics measured between 5 and 300 K.

paramagnetic in the temperature range $T = 5–50$ K. At higher temperatures, such behavior is due to the paramagnetic character of the ferrite $ZnFe_2O_4$, which forms the basis of the iron-rich grains in this ceramics. When the temperature drops to $T \leq 10$ K, the magnetization curves of this sample begin to demonstrate the coercive force H_C reaching 350–450 Oe, which may be caused by the transition of $ZnFe_2O_4$ below 10 K to the antiferromagnetic state.

More complex character of the $M(B)$ is demonstrated by the $(Fe_3O_4)_{10}(ZnO)_{90}$ sample (Fig. 6b), in which the magnetization curves obviously consist of two contributions [35]. The first component is identical to the previous $M(B)$ for $(\alpha\text{-}Fe_2O_3)_{10}(ZnO)_{90}$ ceramics (Fig. 6a) and characterizes the $ZnFe_2O_4$ sub-system, which according to NGR spectroscopy represents more than 70% of the iron-enriched contributions to this ceramics. The second contribution to $M(B)$ curves for $(Fe_3O_4)_{10}(ZnO)_{90}$ sample represents a hysteresis loop with high magnetic susceptibility in low fields and non-zero coercivity (up to 300 Oe) even at room temperature. Such behavior of magnetization curves indicates the ferromagnetic properties of the phase to which they correspond.

Fig. 7 shows the influence of doping on $\rho(T)$ dependences of ceramics in $T > 150–300$ K. As follows from this figure, the doping results in the growth of resostivity of ZnO-based ceramics. In so doing, for all the studied ceramic samples $(Fe_xO_y)_{10}(ZnO)_{90}$ $\rho(T)$ in Arrhenius scale are linear. Moreover they have close values of conduction activation energies $\Delta E_\sigma \approx (0{,}36 \pm 0{,}02)$ eV, which were determined from the slopes of ln $\rho(1/T)$ dependences independently on doping agents.

At the same time, the undoped samples (ZnO) below 300 K were characterized by a “sliding” (non-constant) activation energy of conductance, which decreased upon cooling and did not exceed 0.09 eV in the vicinity of room temperature. The fitting procedure have shown that for $20 < T < 40$ K temperature dependence of $\rho(T)$ obey the Mott relation for Variable Range Hopping conductance (VRH-regime) [35,36]:

$$\rho(T) = \rho_0 \exp[-(T_0/T)^{\alpha}], \quad (1)$$

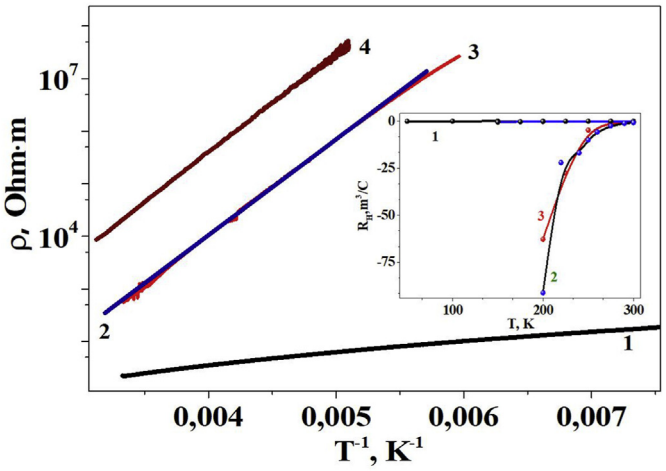

Fig. 7. Temperature dependences of the resistivity $\rho(T)$ in the temperature range of 150–300 K in undoped (1) and doped (2–4) ceramics $(ZnO)_{90}(Fe_xO_y)_{10}$, obtained by the two-step synthesis, doped with FeO (2), α-Fe_2O_3 (3) and Fe_3O_4 (4). Insert: Temperature dependence of Hall constant.

with the optimized parameter $\alpha = 0.25$. The values ρ_0 and T_0 in (1) are fitting parameters of the Mott model (together with α), which determine the probability of electron jumps.

As is seen from Insert in Fig. 7, we could measure Hall constant only for the samples 1-3 with the lowest resistance, and all values of R_H were negative that confirmed the n-type conductance. The log $[n(1/T)]$ dependences in Fig. 8 indicate the presence of two linear parts for low-temperature (with a small slope) and high-temperature (with a large slope). We can attribute such behavior to possible formation of two types of defect centers in wurtzite phase with two different ionization energies. The values of the ionization energies ΔE_i, calculated for these centers from the slopes of the linear regions of the Arrhenius curves in Fig. 8, are equal to 40–90 meV and 0.24–0.35 eV. The values of n near room temperature were between and 9.3×10^{20}, 1.6×10^{19} and 8.2×10^{18} cm^{-3} for ZnO and ceramics doped with FeO and α-Fe_2O_3, correspondingly.

The results of measuring of Seebeck coefficient are presented in

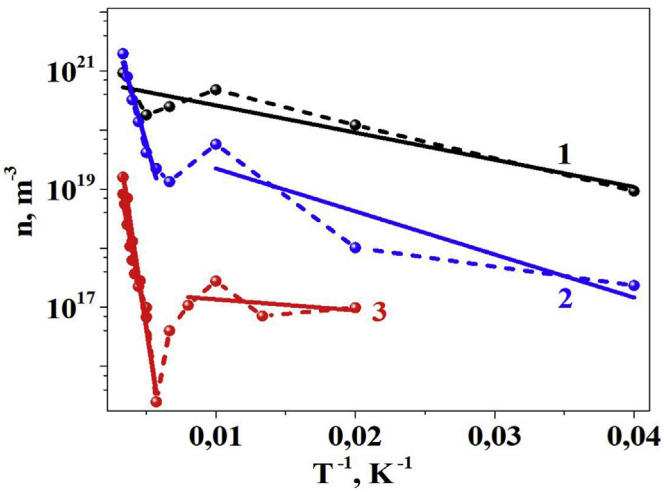

Fig. 8. Temperature dependences of the electron concentration $n(T)$ in the Arrhenius scale for the undoped ZnO (1) and ceramics $(Fe_xO_y)_{10}(ZnO)_{90}$ (1–3) obtained by the two-stage synthesis. Solid straight lines are approximations of linear sections of dependencies. The dashed lines are approximations of experimental dependencies. Points are measurement results for ZnO (1) and ceramics doped with FeO (2), α-Fe_2O_3 (3).

Table 1. As is seen, differential thermo-EMF S_{dif}, was negative that confirms the Hall effect measurements. Taking into account the values of electron concentration n_{300} in the studied ceramics (see, Table 1), we can attribute this effect to the approach of optimal carriers concentration with doping.

5. Summary

The paper proves the influence of the structure, type of doping agents and temperature on the electric and magnetic properties of $(Fe_xO_y)_{10}(ZnO)_{90}$ ($0 \le x \le 3$, $1 \le y \le 4$) ceramics obtained by the method of two-step synthesis on air when commercial powder oxides FeO, Fe_2O_3, and Fe_3O_4 were used as doping agents. X-ray diffraction analysis, EDX measurements, Mossbauer and Raman spectroscopies have shown that in ceramic compositions $(Fe_xO_y)_{10}(ZnO)_{90}$, at least three phases were formed: wurtzite $Zn_{1-\delta}Fe_\delta O$ with iron content $\delta \le 0.81$ at. %, ferrite $ZnFe_2O_4$ with a spinel structure, as well as residual iron oxides Fe_xO_y. The SEM method allowed to find that the grain sizes of the wurtzite phase in the studied ceramics decrease from several tens of micrometers using one-step synthesis to the submicron level for the case of the two-step synthesis. The use of two-step synthesis also leads to an increase in the homogeneity of the distribution of grains in size and composition.

It was found that compaction and two-stage annealing of powder mixtures $(\alpha\text{-}Fe_2O_3)_{10}(ZnO)_{90}$ result in a ceramic with paramagnetic properties at room temperature. This is associated with the ferrite $ZnFe_2O_4$ formed in $(\alpha\text{-}Fe_2O_3)_{10}(ZnO)_{90}$ ceramics. At $T \le 10$ K, $ZnFe_2O_4$ has an increased coercive force (350–450 Oe), which is due to its transition to an antiferromagnetic state. The use of Fe_3O_4 as a doping agent leads to the formation of ceramics, which has weak ferromagnetic properties at room temperature due to the presence of residual α-Fe_2O_3 phase, which contributes to an increase in magnetic susceptibility and coercive ceramics forces (up to 300 Oe) at room temperature.

As was found from Hall effect and resistivity measurements, the introduction of iron into the wurtzite ZnO phase, in addition to shallow donors with an ionization energy of about 50–90 meV, forms deep donor centers with the ionization energy of 0.24–0.36 eV and an activation energy of conduction of about 0.35 eV. The values of electron concentration near room temperature are between and 9.3×10^{20}, 1.6×10^{19} and 8.2×10^{18} cm^{-3} for ZnO and ceramics doped with FeO and α-Fe_2O_3, correspondingly. The temperature dependences of the electrical resistance $\rho(T)$ in the undoped zinc oxide in the temperature range of 6–300 K are characterized by a variable activation energy, which indicates a highly disordered structure in it. It was shown by fitting procedure that at $20 < T < 40$ K the $\rho(T)$ obey the Mott law for variable range hopping conductance.

We believe that the results presented in this article clarify the understanding by researchers how and what phases are formed in composites based on zinc oxide obtained by ceramic technology. Further studies will be directed to the use of more complex doping and structuring of ceramics of this kind, which will reduce their electrical conductivity and thermal conductivity while maintaining the detected enhancement of the Seebeck effect when alloyed with iron.

Table 1
Seebeck effect in the ceramic samples $(Fe_xO_y)_{10}(ZnO)_{90}$ with $0 \le x \le 3$, $1 \le y \le 4$).

Sample	$-S_{dif}$, μV/K	n_{300}, cm^{-3}
ZnO	375–396	9.3×10^{20}
$(ZnO)_{90}(FeO)_{10}$	723–752	1.6×10^{19}
$(ZnO)_{90}(Fe_2O_3)_{10}$	762–773	8.2×10^{18}
$(ZnO)_{90}(Fe_3O_4)_{10}$	809–861	–

CRediT authorship contribution statement

A.K. Fedotov: Participation in Writing - review & editing. **A.V. Pashkevich:** Participation in, Investigation. **J.A. Fedotova:** Conceptualization. **A.S. Fedotov:** Software. **T.N. Kołtunowicz:** Conceptualization, Corresponding Author, Funding acquisition. **P. Zukowski:** Participation in Writing - review & editing, Funding acquisition. **Ali Arash Ronassi:** Methodology. **V.V. Fedotova:** Data curation. **I.A. Svito:** Participation in Investigation. **M. Budzyński:** Validation.

Declaration of competing interest

The authors declare that they have no known competing financial interests or personal relationships that could have appeared to influence the work reported in this paper.

Acknowledgments

The authors thank the State Program of scientific research "*Physical Materials Science, New Materials and Technologies*" (Belarus) for the financial support.

This research was partially funded from the Polish Ministry of Science and Higher Education from science fund of the Lublin University of Technology, at the Faculty of Electrical Engineering and Computer Science FN-28/E/EE/2019, entitled "*Researches of electrical, magnetic, thermal and mechanical properties of modern electrotechnical and electronic materials, including nanomaterials and diagnostic of electrical devices and their components*".

The authors thank Ph.D. O.V. Korolik for carrying out Raman spectroscopy of the samples under study.

Appendix A. Supplementary data

Supplementary data to this article can be found online at https://doi.org/10.1016/j.jallcom.2020.156169.

References

[1] L.M. Levinson, Ceramic Transactions, Grain Boundaries and Interfacial Phenomena in Electronic Ceramics vol. 41, American Ceramic Society, Westerville, OH, 1994.
[2] A. Sawalha, M. Abu-Abdeen, A. Sedky, Physica B 404 (2009) 1316–1320.
[3] D. Winarski, Synthesis and Characterization of Transparent Conductive Zinc Oxide Thin Films by Sol-Gel Spin Coating Method, Thesis of master science, College of Bowling Green State University, 2015.
[4] V.R. Kopach, K.S. Klepikova, N.P. Klochko, G.S. Khrypunov, V.E. Korsun, V.M. Lyubov, M.V. Kirichenko, A.V. Kopach, Sov. Phys. Semiconduct. 51 (3) (2017) 335–343.
[5] M.G. El-Shaarawy, M. Khairy, M.A. Mousa, Adv. Powder Technol. 31 (3) (2020) 1333–1341.
[6] Y. Nose, T. Yoshimura, A. Ashida, T. Uehara, N. Fujimura, J. Soc. Mater. Sci. Jpn. 61 (2012) 756–759.
[7] A.D. Pogrebnyak, N.Y. Jamil, A.K.M. Mohammed, Metallofiz. Noveishie Tekhnol. 33 (2011) 235–241. Spec. Iss.
[8] A. Turlybekuly, A.D. Pogrebnjak, L.F. Sukhodub, L.B. Sukhodub, A.S. Kistaubayeva, I.S. Savitskaya, D.H. Shokatayeva, O.V. Bondar, Z.K. Shaimardanov, S.V. Plotnikov, B.H. Shaimardanova, I. Digel, Mater. Sci. Eng. C 104 (2019) 109965.
[9] J.R. Bellingham, W.A. Phillips, C.J. Adkins, J. Mater. Sci. Lett. 11 (1992) 263–265.
[10] A. Pogrebnjak, A. Muhammed, E. Karash, N. Jamil, J. Partyka, Przeglad Elektrotechniczny 89 (3B) (2013) 315–317.
[11] T.A. Krajewski, K. Dybko, G. Luka, L. Wachnicki, K. Kopalko, W. Paszkowicz, M. Godlewski, E. Guziewicz, J. Appl. Phys. 118 (2015) 35706.
[12] A. Di Trolio, P. Alippi, E.M. Bauer, G. Ciatto, M.H. Chu, G. Varvaro, A. Polimeni, M. Capizzi, M. Valentini, F. Bobba, C. Di Giorgio, A. Amore Bonapasta, ACS Appl. Mater. Interfaces 8 (2016) 12925–12931.
[13] S. Niki, K. Matsubara, H. Tampo, K. Nakahara, J. Vac. Soc. Jpn. 50 (2017) 40–43.
[14] D. Gaspar, L. Pereira, K. Gehrke, B. Galler, E. Fortunato, R. Martins, Sol. Energy Mater. Sol. Cells 163 (2017) 255–262.
[15] A.M. Ismailov, V.A. Nikitenko, M.R. Rabadanov, L.L. Emiraslanova, I.S. Aliev, M.K. Rabadanov, Vacuum 168 (2019). UNSP 108854.
[16] C. Li, M. Furuta, T. Matsuda, T. Hiramatsu, H. Furuta, T. Hirao, Thin Solid Films 517 (2009) 3265–3268.
[17] M. Xia, Z.-F. Cheng, J. Han, M. Zheng, C.-H. Sow, J.T.L. Thong, S. Zhang, B. Li, AIP Adv. 4 (2014) 57128.
[18] D. Raoufi, Renew. Energy 50 (2013) 932–937.
[19] N. Shimoi, T. Harada, Y. Tanaka, S.-I. Tanaka, AIP Adv. 2 (2012) 22167.
[20] H.N. Sahu, B.N. Sherikar, Int. J. Eng. Res. Technol. 6 (2) (2017) 591–596.
[21] D. Chiba, N. Shibata, A. Tsukazaki, Sci. Rep. 6 (2016) 38005.
[22] M. Mustaqima, C. Liu, Turk. J. Phys. 38 (2014) 429–441.
[23] S.J. Pearton, D.P. Norton, Y.W. Heo, L.C. Tien, M.P. Ivill, Y. Li, B.S. Kang, F. Ren, J. Kelly, A.F. Hebard, J. Electron. Mater. 35 (5) (2006) 862–868.
[24] H.J. Goldsmith, Introduction to the Thermoelectricity, second ed., Springer, 2016.
[25] D.M. Rowe, Handbook of Thermoelectrics, CRC Press, Boca Raton, 1995.
[26] J. Rodriguez-Carvajal, Physica B 192 (1993) 55–69.
[27] D.G. Rancourt, Nucl. Instrum. Methods Phys. Res. Sect. B Beam Interact. Mater. Atoms 44 (1989) 99–210.
[28] Powder Diffraction, Joint Committee on Powder Diffraction Standards, ICDD, Newtown Square, 2001.
[29] M. Silambarasan, S. Saravanan, T. Soga, *Raman and photoluminescence Studies of Ag and Fe-doped ZnO*, International Conference on Nanoscience and Nanotechnology-2015, SRM University, Chennai, India, Int. J. ChemTech Res. 7 (3) (2014-2015) 1644–1650.
[30] P. Zou, X. Hong, X. Chu, Y. Li, Y. Liu, J. Nanosci. Nanotechnol. 10 (2010) 1992–1997.
[31] A. Roychowdhury, A.K. Mishra, S.P. Pati, D. Das, AIP Conf. Proc. 1447 (2012) 283–284.
[32] X.L. Wu, G.G. Siu, C.L. Fu, H.C. Ong, Appl. Phys. Lett. 78 (16) (2001) 2285–2287.
[33] A.R. Vazquez-Olmos, M. Abatal, R.Y. Sato-Berru, G.K. Pedraza-Basulto, V. Garcia-Vazquez, A. Sainz-Vidal, R. Perez-Bañuelos, A. Quiroz, J. Nanomater. 2016 (2016) 9182024.
[34] L.I. Granone, A.C. Ulpe, L. Robben, S. de Klimke, M. Jahns, F. Renz, T.M. Gesing, T. de Bredow, R. Dillert, D.W. Bahnemann, Phys. Chem. Chem. Phys. 20 (2018) 28267–28278.
[35] N.F. Mott, E.A. Davis, Electronic Processes in Non-crystalline Materials, second ed., Clarendon, Oxford, 1979.
[36] V.I. Shklovski, A.L. Efros, Electronic Properties of Doped Semiconductors, Springer-Verlag, 1984.